Abstract

The conditions created by breaking waves in the ocean are turbulent and complex, and the mixing driven by this turbulence has a great impact on the fate of contaminants in the water. Numerical simulations can help illuminate these conditions, as well as being tools for predicting the development of such systems.

A comparison of two stochastic particles methods: random walk and random flight, have also been made. They were found to preform similarly in their abilities to satisfy the well-mixed condition, in their order of convergence in both the strong and weak sense, and in their Monte Carlo error.

A comparison of a simple reflection scheme and a more involved scheme presented by Lépingle (1995) in random walk methods have been made. It was found that the Lépingle method, in addition to being computationally more expensive, also performs worse than the simple scheme at reflecting boundaries with non-zero derivative of the diffusivity profile. It was also found to have a lower order of convergence, and a poorer ability to preserve the well-mixed state of a diffusion system in line with the well-mixed condition presented by Thomson (1987).

Samandrag

Forholda som vert skapt av brytande bølgjer i havet er turbulente og samansette, og blandinga drevet av denne turbulensen har stor innverknad på skjebnen til t.d. forureining i vatnet. Numeriske simuleringar kan bidra til å kaste lys på disse forholda, i tillegg til å vere verktøy for å føreseia utviklinga av slike system.

Ei samanlikning av to stokastiske partikkelmetodar: virrevandring og tilfeldig flukt, har også verte gjort. Dei vart funne å prestere likt på evna deira til å tilfredsstille godt-blanda-kriteriet, konvergensordenen deira i både sterk og svak forstand, og i Monte Carlo-feilen deira.

Det har vorte gjort ei samanlikning av ein enkel refleksjonsmetode og ein meir involvert metode presentert av Lépingle (1995) i virrevandringsmetodar. Det vart funne at Lépingle-metoden, i tillegg til å vere berekningsmessig dyrare, også presterte dårlegare enn den enkle metoden ved reflekterande grenser med ikkje-null-derivert diffusivitetsprofil. Den vart også funne å ha ein lågare konvergensorden, og ei dårligare evne til å bevare den godt blanda tilstanden til eit diffusjonssystem i tråd med godt-blanda-kriteriet presentert av Thomson (1987).

Preface

This thesis was written during my last year of the MSc program in Physics at NTNU, during the autumn semester of 2022 and spring semester of 2023. The work presented is part of the project ENTIRE at SINTEF Ocean, and is situated within the field of numerical physics.

 The files used to compile this document can be found in my Git repository[2]. Corrections and inquieries can be sent to konrad.jervell@ntnu.no. The software created to run the simulations is free software published under the GNU General Public License Version 3[3] and the code can be found in my public Git repository[4].

Acknowledgements

I firstly want to thank my supervisor, Dr. Tor Nordam, who has greatly aided me in this work, not only with his knowledge of the field in which this thesis is situated, but also his ability to communicate and explain concepts of differing complexity in an intuitive, understandable, and pedagogical way. Without his mentoring and support the work presented here would not have been possible.

I also want to thank my friends Anders A. Tidemann and Elias O. Slettevoll for their collaboration though all our years studying together, and for the thoughtful and inspirational conversations we have had.

A thank should also be extended to my comrades in Δp for all the memories that will last a lifetime. May you continue to be the vanguard that you are!

My family also deserves a thanks; especially my parents Monica and Halvard Jervell, for both letting and helping me pursue whatever my curiosity lead me to. This work would not have been possible without you.

Lastly I want to thank my wonderful girlfriend, Frida H. Carpenter, for her support and infinite kindness and patience. Our conversations and jokes have kept me afloat this last year.

[1] https://creativecommons.org/licenses/by-nc-sa/4.0/legalcode
[2] https://codeberg.org/konki/master_thesis
[3] https://www.gnu.org/licenses/gpl-3.0
[4] https://codeberg.org/konki/Masterprosjekt

Contents

List of Figures

List of Symbols

Physical system parameters

L	Total depth of water column
z	Vertical position in the water column
$K(z)$	Diffusivity as a function of depth

Simulation parameters

Np	Total number of tracked particles in a simulation
Δt	Timestep used in a simulation
T	Total runtime of simulation
ΔW	An increment of the Wiener-process

Abbrevations

SDE	Stochastic differential equation
PDE	Partial differential equation
FDM	Finite difference method
WMC	Well mixed condition
PDF	Probability density function
MAE	Mean absolute error
AE	Absolute error
RMSE	Root mean square error

Chapter 1

Introduction

1.1 History

The phenomenon of diffusion has fascinated scientists for centuries, and it has been studied extensively in various contexts. A significant observation was made in 1827, when the Scottish botanist Robert Brown observed the erratic motion of pollen particles suspended in water under a microscope. The motion seemed so life-like that he thought it had to be the result of some life-force within the pollen, but after repeating the experiment with small particles of inorganic minerals and observing the same erratic motion, he concluded that the source could not be related to life, but its source still remained a mystery.

A breakthrough was made in 1905 when Albert Einstein published one of his four influential papers in his *annus mirabilis*. His second paper of the year outlaid a theoretical framework for the description of Brownian motion and linked it to the then much disputed kinetic theory of gasses (Einstein, 1905). The paper presented an expression for the mean square displacement of particles undergoing Brownian motion, and this expression together with simple observations of such motion under a microscope made it possible for physicists and chemists to calculate such fundamental constants to those fields as the Boltzmann constant and Avogadro's number.

Measurements of the mean square displacement of particles undergoing Brownian motion were later made by Jean Baptiste Perrin in 1909 and presented in his paper *Brownian motion and molecular reality* (Perrin, 1909). This was the first time researchers had been able to directly calculate the masses of atoms and molecules, and Perrin was awarded the Nobel Prize in Physics in 1926 largely for this work. (NobelPrize.org, 2023)

At the same time, the French physicist Paul Langevin developed an equation for the description of the movement of particles undergoing Brownian motion (Langevin, 1908). The Langevin equation, which is essentially Newton's second law with a drag

force and a random agitating force, became an early example of what we today call stochastic differential equations. The term "Langevin equation" is now often used more generically as a name for any equation describing fast random fluctuations in a slowly changing system (see e.g. Coffey and Kalmykov (2012)). The theory of SDEs was later, in the 1940s, developed by Japanese mathematician Kiyosi Itô into the field of Itô calculus which extends the methods of calculus to the realm of stochastic processes.

The observations made and tools developed by these pioneering scientists made way for more modern applications with the advent and greater availability of computers. For instance do random walk methods, which may be constructed from discretization of the Langevin equation, have a long history of applications in the modelling of oil spill transport, both vertically (Tayfun and Wang, 1973) and horizontally (Elliott et al., 1986), as well as the transport of plastics in the ocean (Onink et al., 2021), and airborne transport of viruses (Abuhegazy et al., 2020).

1.2 Motivation

The conditions created by breaking waves in the ocean are complex and dynamic, making them a challenging area of study. One particular aspect of interest is the mixing driven by breaking waves. As waves break, they create turbulence and mixing in the water column, which can enhance the transport and dispersion of dissolved substances such as nutrients, pollutants, and gasses, or other substances such as harmful plankton. The resulting diffusion process can have significant implications for the ecology and biogeochemistry of the ocean, as well as for the fate of pollutants and contaminants. Understanding the mechanisms and dynamics of diffusion driven by breaking waves is therefore crucial for predicting and mitigating the impact of human activities on the marine environment.

The simulation of movement of particles in the ocean is an important tool both for researchers, but also for agencies tasked with responding to contamination of seawater from e.g. oil spills. Moreover, the absorption of carbon dioxide in the ocean is to a large extent driven by entrainment of bubbles facilitating the contact of the CO_2 with water from further down in the water column which might be less saturated. In all these cases the entrainment of the particles in the water is of special interest since it greatly affects the overall dynamics of the system.

There are two main approaches when one seeks to study fluid flow numerically: The Eulerian approach, which considers the vector field of fluid motion, and the Lagrangian approach, which simulates a number of tracer particles individually. When using the latter approach one is free to choose how many time derivatives of

the position is taken into consideration: The most common approach is to simply consider the position of the particles with no regard to the velocity and higher order time derivatives. An alternative approach is to consider both the position and velocity of the particle, still disregarding the higher order time derivatives of the position such as acceleration (see e.g. Lynch et al. (2014, chapter 4)). One of the goals of this thesis is to compare these two different approaches in modelling the turbulent diffusion of particles in water.

It is also a known issue (Ross and Sharples, 2004; Nordam et al., 2019) with Lagrangian models that they might produce artifacts near certain reflecting boundaries, though the issue of boundary conditions in random walk methods have received limited attention in the applied literature. This thesis will investigate an alternative reflection scheme as presented by Lépingle (1995) which might perform better than the traditional approach.

1.3 Outline of the thesis

This thesis is structured around chapters where the first chapter following this one will present the necessary equations and theoretical background for the following chapters. Next, in chapter 3, I will present the methodology used to find the results which will be presented along with a discussion in chapter 4. Finally, in chapter 5, I present the conclusions drawn from the results and discussions in chapter 4. At the end of this thesis in appendix A I give a proof of the stability of the Crank-Nicolson method.

Chapter 2

Theory

This chapter will present the theoretical foundations that will be used in the investigations later in this thesis. Throughout the whole thesis we will consider a one-dimensional system representing a water column with positive z-direction downwards, and $z = 0$ located at the water surface.

2.1 Diffusion processes

Diffusion can generally be thought of as the process of particles moving from areas of high concentration to areas of lower concentration. This process can happen on different scales based on the conditions of the system. The two main modes of diffusion are molecular and turbulent. The prior is driven by the thermal kinetic energy of the particles as a result of temperature, while the latter is a result of more macroscopic movement of the solvent fluid (Thorpe, 2005, pp. 20-21). Molecular diffusion is generally considered negligible in systems where turbulent diffusion also occurs since its scale is much smaller, and this thesis will only focus on the latter mode of diffusion.

In the one dimensional case, vertical transport may be described by the following equation, simply called the *advection-diffusion equation*:

$$\frac{\partial C}{\partial t} = \frac{\partial}{\partial z}(-\omega C + K\frac{\partial C}{\partial z}), \tag{2.1}$$

where C is the concentration of the particles of interest, z is the vertical position, t is time, ω is the advection and K is the diffusivity of the solvent fluid. In the case of no advection, $\omega = 0$, equation (2.1) simplifies to the *diffusion equation*

$$\frac{\partial C}{\partial t} = \frac{\partial K}{\partial z}\frac{\partial C}{\partial z} + K\frac{\partial^2 C}{\partial z^2}. \tag{2.2}$$

While the concentration is a macroscopic and deterministic quantity, it is the result of the small-scale and largely stochastic movements of the particles of interest. This stochastic nature of diffusion can be expressed with a stochastic differential equation (SDE) describing the development of the position of the tracer particles. Such an equation can be constructed to describe the same system as the partial differential equation (PDE) in equation (2.1) via the Fokker-Planck equation. The Fokker-Planck equation and resulting SDE will be discussed in the following sections.

2.2 Markov processes

A process $X(t)$ which depends on the real variable t, representing time, is said to be *Markov* or *Markovian* if the state of the process in the future only depends on the current state of the process, and not directly on any states prior to the present. This property is called the Markov property, and can be thought of as the process being memoryless or past-forgetting. This is not to say that the process is independent of the past states, but that the future state only depends on the past through that of the past that is represented in the present (Gillespie and Seitaridou, 2012, p. 149). The numerical methods we will discuss later in sections 2.6 and 2.7 for the simulation of diffusion are both examples of Markov processes.

2.3 The Langevin equation

In 1908 the French physicist Paul Langevin developed an equation to describe the movement of a particle undergoing Brownian motion

$$m\frac{\mathrm{d}^2x}{\mathrm{d}t^2} = -6\pi\mu a\frac{\mathrm{d}x}{\mathrm{d}t} + X. \tag{2.3}$$

The equation emerges from Newton's second law where the two terms on the right are the viscous drag force and some stochastic agitating force respectively. About the agitating force X, Langevin said that "[...] *we know that it is indifferently positive and negative and that its magnitude is such that it maintains the agitation of the particle, which the viscous resistance would stop without it.*" (Lemons and Gythiel, 1997). We will later look at a stochastic process which satisfies this criterion when we consider the Wiener process in section 2.5.

Equation (2.3) is an example of what is now called a stochastic differential equation, a concept we will return to in the following sections. What this means is that we have a differential equation where at least one of the terms is a stochastic process; in the case of the original Langevin equation: the agitating force X. A typical SDE

can be written on the form

$$dz(t) = a(z(t), t)dt + b(z(t), t)dW_t, \tag{2.4}$$

where $a(z(t), t)$ and $b(z(t), t)$ are called the drift- and diffusion coefficients respectively, and W_t is a stochastic process called *the Wiener process*, which we mentioned earlier and will return to in section 2.5.

The Langevin equation was so influential in the development of the concept of SDEs that we now often call any SDE describing the fast random fluctuations in a system whose average properties change only slowly a Langevin equation, with equation (2.3) itself being called the *original* Langevin equation. This is the terminology we will use going forward in this thesis.

2.4 Fokker-Planck equation

The Fokker-Planck equation of a system describes the temporal evolution of the probability distribution of some attribute of that system. Commonly it describes the development of the probability distribution of either the velocity or position of particles undergoing Brownian motion. Equation (7.14) in Kloeden and Platen (1992, p. 37) gives us the Fokker-Planck equation for a diffusion process $dz = a(z, t)dt + b(z, t)dW$:

$$\frac{\partial p}{\partial t} + \frac{\partial}{\partial z}(a(t, z)p) - \frac{1}{2}\frac{\partial^2}{\partial z^2}(b^2(t, z)p) = 0, \tag{2.5}$$

where a and b are the drift- and diffusion coefficients respectively. This equation then describes the temporal development of the probability distribution for the position of the particles in the diffusion process. The development of this probability distribution is fully deterministic, but as mentioned before, equation (2.5) can be utilized to find an SDE that describes the same system as the PDE in equation (2.1). Before presenting this SDE we will first introduce the Wiener process which will be utilized extensively in the following chapters.

2.5 The Wiener process

The Wiener process, denoted $W(t)$ or W_t, is a continuous stochastic process over time that exhibit the following characteristics:

1. $W(0) = 0$; Its values are initialized as 0,
2. $W(t)$ is continuous over time t,

3. Its non-overlapping increments $W(t + dt) - W(t) = dW_t$ are independent of each other,

4. $dW_t = W(t + dt) - W(t) = \mathcal{N}(0, dt)$; The increment between two states is normally distributed with mean 0 and variance dt .

This process is a generalization to continuous time of the fixed-stepsize random walk where at each timestep the process takes a fixed step in a random direction. Figure 2.1 is a simple illustration of the two processes. We will mainly be concerned with

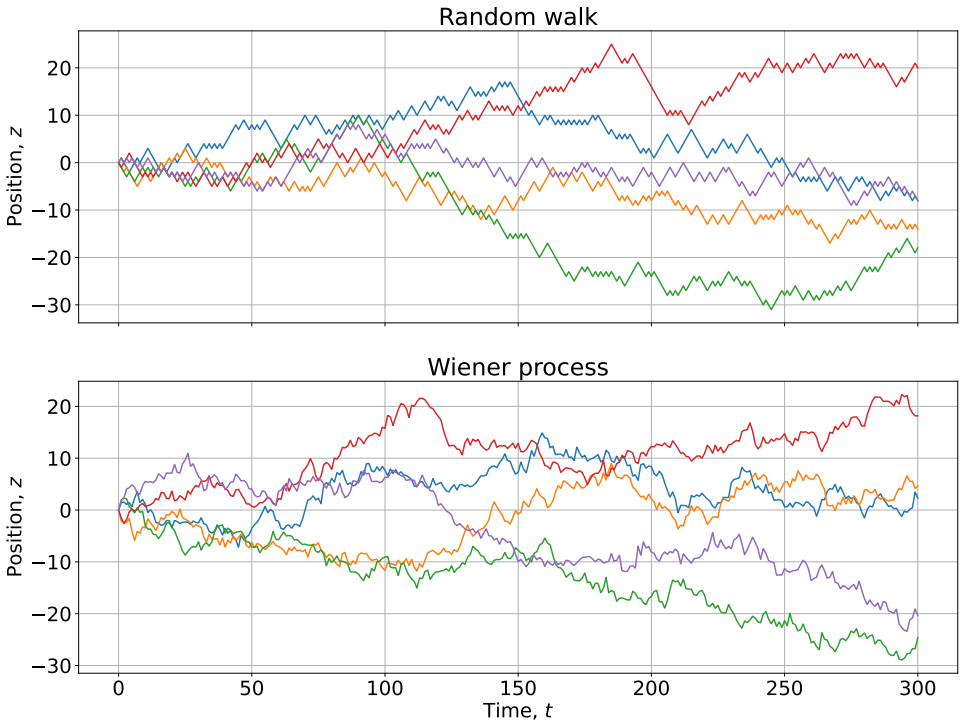

Figure 2.1: Five realizations of a fixed-stepsize random walk and five realizations of the Wiener process. The units on both axes are arbitrary.

the increment dW of the Wiener process as it will play a central role in the SDEs that are to be presented next.

2.6 Random walk

Building on the previous sections we will now introduce a random walk scheme for the simulation of turbulent mixing. In contrast to the fixed-stepsize random walk mentioned in section 2.5 this random walk will have a variable stepsize, and be

constructed to represent a diffusion system. According to equation (2) in Gräwe et al. (2012) the SDE describing the diffusion system of equation (2.1) is

$$dZ(t) = \left(\omega + \frac{\partial K}{\partial z}\right) dt + \sqrt{2K(z)} dW(t) \tag{2.6}$$

where $a(t,z) = \omega + \frac{\partial K}{\partial z}$ and $b(t,z) = \sqrt{2K(z)}$, and $dW(t)$ is an increment of the Wiener process as defined in section 2.5. Inserting these expressions for a and b into the Fokker-Planck equation given in equation (2.5), we get

$$\begin{aligned}
& \frac{\partial p}{\partial t} + \frac{\partial}{\partial z}\left(\left(\omega + \frac{\partial K}{\partial z}\right) p\right) - \frac{1}{2}\frac{\partial^2}{\partial z^2}\left(\left(\sqrt{2K(z)}\right)^2 p\right) = 0 && (2.7)\\
\Rightarrow \quad & \frac{\partial p}{\partial t} = -\frac{\partial}{\partial z}\left(\omega p + \frac{\partial K}{\partial z} p\right) + \frac{\partial^2}{\partial z^2}\left(K(z) p\right) \\
\Rightarrow \quad & \frac{\partial p}{\partial t} = \frac{\partial}{\partial z}\left(-\omega p - \frac{\partial K}{\partial z} p\right) + \frac{\partial}{\partial z}\left(\frac{\partial K}{\partial z} p + K\frac{\partial p}{\partial z}\right) \\
\Rightarrow \quad & \frac{\partial p}{\partial t} = \frac{\partial}{\partial z}\left(-\omega p + K\frac{\partial p}{\partial z}\right). && (2.8)
\end{aligned}$$

If we then consider that p is the probability distribution of the particle positions, which is equivalent to the normalized concentration, and do the substitution $p \to C$, equation (2.8) simply becomes the advection-diffusion equation from equation (2.1), showing us that this random walk scheme indeed is a represetntation of the system in equation (2.1).

Equation (2.6) represents the change in the particle positions over time, and we observe that for stationary diffusivity K and advection ω the only temporal dependence of the increment is in $dW(t)$.

Another observation to make is that if equation (2.6) represents a change in spatial position of the particle, and this change takes place over a time interval dt, one might ask what the resulting velocity of the particle is. One might be inclined to derive the velocity by dividing both sides by dt giving

$$\frac{\mathrm{d}Z}{\mathrm{d}t} = \left(\omega + \frac{\partial K}{\partial z}\right) + \sqrt{2K(z)}\frac{\mathrm{d}W(t)}{\mathrm{d}t}, \tag{2.9}$$

but given that

$$dW(t) = \mathcal{N}(0, dt) = \sqrt{dt}\mathcal{N}(0,1) \tag{2.10}$$

from item 4 in section 2.5, equation (2.9) becomes

$$\frac{\mathrm{d}Z}{\mathrm{d}t} = \left(\omega + \frac{\partial K}{\partial z}\right) + \sqrt{2K(z)}\frac{\mathcal{N}(0,1)}{\sqrt{dt}}. \tag{2.11}$$

We observe that in the limit $dt \to 0$, the last term on the right-hand side of equation (2.11) diverges due to the term $\sqrt{dt}$ that remains in the denominator. This results in infinite velocity, which is obviously unphysical, and we will return to this problem and a possible solution in section 2.7 where we look at *random flight*. As we will see later, infinitely fast transport is also a feature of the diffusion equation, with which equation (2.6) is consistent.

Going forward, we will consider systems where the advection $\omega = 0$, meaning we will consider systems of pure diffusion. If we discretize equation (2.6) using the Euler-Maruyama method (Kloeden, 1992, p. 305) we get a discrete updating formula for position that we will utilize in the Lagrangian model that we will look at later.

$$z_{n+1} = z_n + K'(z)\Delta t + \sqrt{2K(z)}\Delta W_n, \tag{2.12}$$

where $K'(z) = \frac{\partial K}{\partial z}$, and $n \in \{0, 1, ..., T/\Delta t\}$ is the discrete temporal index of a given spatial state z. The two last terms of the right-hand side are discrete steps in space, and are often collected in a single term

$$\Delta z = K'(z)\Delta t + \sqrt{2K(z)}\Delta W_n. \tag{2.13}$$

These equations represent a scheme for simulating the development of the position of a particle over time given some initial position z_0 which is called a *random walk* method, and it is widely used in simulating diffusive mixing due to its simplicity.

2.7 Random flight

One solution to the unphysicalness of the velocity of the traced particles resulting from the random walk method is to use a different method where we consider the velocity directly. We will call such a model, where the velocity is given by an SDE, a *random flight* model. An expression for the Langevin equation can be found in model 2 in Griffa (1996) which considers a joint Markovian process x and u (in this thesis labeled z and v). Modifying equation (7) in Griffa to use our notation we get

$$dV(t) = -\frac{1}{\tau}V(t)dt + \sqrt{\frac{K(Z)}{\tau^2}}dW(t), \tag{2.14}$$

where we have done the substitution $T \to \tau$. Here V represents the velocities of the particles at a given time t and $dW(t)$ is the increment of the familiar Wiener process. τ is the so called *decorrelation time* or *relaxation time* which describes the time it takes for the particle to "forget" its previous velocity. The first term on the right-hand side, in which τ participates inversely, represents the drag force which

leads to this loss of memory of the velocity.

This model is equivalent to the Ornstein-Uhlenbeck process, and the Fokker-Planck equation of this process with constant diffusivity K can be found in equation (1.5) in Gillespie (1996)

$$\frac{\partial p}{\partial t} - \frac{1}{\tau}\frac{\partial [vp]}{\partial v} - \frac{K}{2}\frac{\partial^2 p}{\partial v^2} = 0. \tag{2.15}$$

Given the Langevin equation for the velocity in equation (2.14), a very simple physical argument can be made for writing the Langevin equation of the position in this scheme as

$$dZ(t) = V(t)dt. \tag{2.16}$$

It is important to note that in this model, Z and V are no longer Markovian on their own as V is not memoryless, but jointly they still satisfy the condition for being Markovian.

Applying Euler-Maruyama to equations 2.14 and 2.16 we find the discrete updating formula for the random flight

$$v_{n+1} = v_n + \Delta v \tag{2.17}$$

$$z_{n+1} = z_n + v_n \Delta t \tag{2.18}$$

where $n \in \{0, 1, ..., T/\Delta t\}$ again is the discrete temporal index of a given state, and

$$\Delta v = -\frac{1}{\tau} v_n \Delta t + 2\sqrt{\frac{K(z_n)}{\tau^2}} \Delta W_n. \tag{2.19}$$

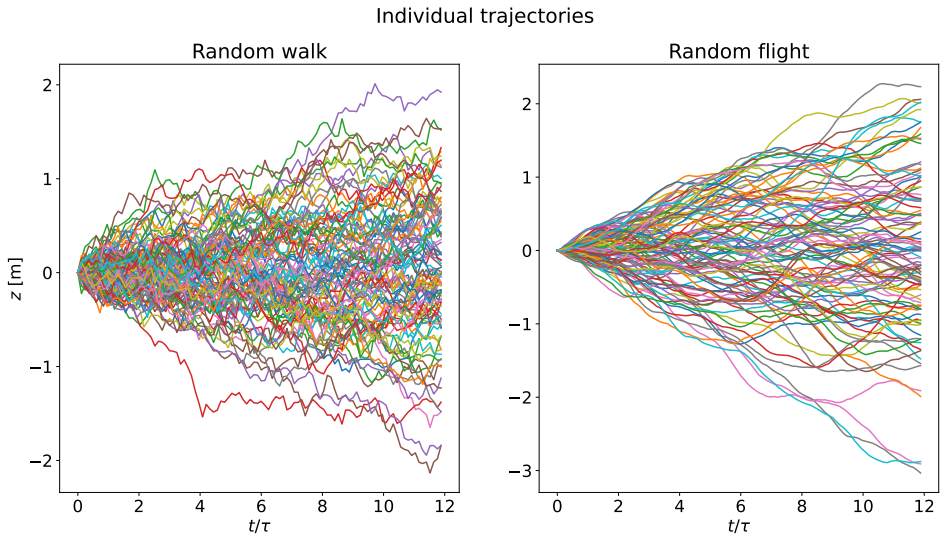

Figure 2.2: Trajectories of random walk and random flight on short timescales.

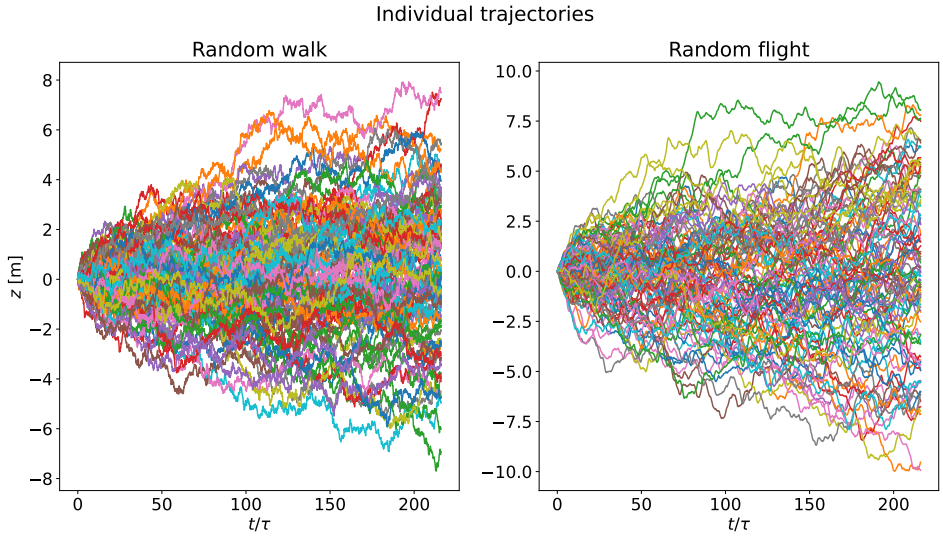

Figure 2.3: Trajectories of random walk and random flight on long timescales.

When particles are simulated using the random flight method, we expect that their trajectories become "smooth" since they will have a tendency to keep travelling in the same direction as they did before. This is precisely what is shown in figure 2.2 where particle trajectories from a random walk and random flight are compared on a short timescale. "Short" in this context means that the relative time $\frac{t}{\tau}$ is small. On longer timescales however, we expect the effects of the memory of the velocity to diminish, and for the trajectories to become more "jagged" and more similar to those of the random walk. This is illustrated in figure 2.3. This motivates us to guess that the choice between these two methods plays a bigger role on short time scales than on long ones.

The jaggedness of the random walk is due to the Wiener process itself being jagged, which is a result of its pathological quality of being continuous everywhere but differentiable nowhere. The non-differentiability of the Wiener process was implicitly seen when we observed that the right-hand side of equation (2.11) diverges when $dt \to 0$. Physically this relates to the discussion about the velocity of the random walk where we saw that it changes quickly and could become very large.

2.7.1 Properties of random flight velocity

Some properties of the random flight method that might be worth investigating are the autocorrelation of the velocity, and how the velocity distribution develops over long times.

The former describes how the velocity at a given timestep is correlated with the velocity at all other timesteps, or in other words; how much the velocities are coupled

over time. Equation (9) in Griffa (1996) gives the theoretical autocorrelation of the velocity of the random flight model as

$$R(t) = \frac{\langle v(\tilde{t})v(\tilde{t}+t)\rangle}{\sigma} = e^{-t/\tau} \tag{2.20}$$

where σ is the standard deviation of the initial velocity distribution, which is assumed to be normal and centered at 0.

It can be found from the Fokker-Planck equation (2.15) that for any time $t > 0$ the velocity distribution $V(t)$ will be normally distributed with mean and variance

$$\langle V(t)\rangle = v_0 e^{-t/\tau} \tag{2.21}$$

$$\mathrm{Var}(V(t)) = \frac{K\tau}{2}(1 - e^{-2t/\tau}), \tag{2.22}$$

where v_0 is the initial velocity and K is assumed constant (equations (2.2) and (2.3) Gillespie, 1996). If we want to know the behavior of the velocity on long time scales, we simply take the limits of the above equations as $t \to \infty$, which clearly shows that the mean and variance approach 0 and $\frac{K\tau}{2}$ respectively.

2.8 Eulerian and Lagrangian modelling

As mentioned in the introduction there are two main ways of simulating mixing due to fluid flow numerically where the first, Eulerian, considers each position on a finite grid and how a conserved quantity, such as particle concentration, develops at these positions given some vector field describing the flow and a parameter describing the diffusivity. These methods require a fixed position grid and may be solved using a *finite difference method* (FDM). This involves setting up a linear algebra system and solving it for each timestep; something computers are very efficient at doing. This method, however, does not include a notion of singular particles, and it is therefore not possible to consider an ensemble where different particles in the same position can have different velocities since the velocity at a given position is determined by the vector field.

The Lagrangian models, on the other hand, track individual particle packets or parcels. This lets us track any number of properties of these particles, such as both position and velocity, and these properties can vary continuously inside some predefined range. Here, each parcel is simulated and tracked through the entire diffusion process. These methods do not require a discretization of the space since the position of the particles can vary continuously (to the precision of the computer on which the simulation is run). However, it is often unpractical to simulate

inter-particle interactions and these are therefore often neglected for large particle ensembles.

In both cases we simulate the mixing with the assumption of knowing the necessary characteristics of the overall fluid flow.

2.8.1 A suitable FDM

An example of an FDM that is well suited for solving the diffusion equation is the Crank-Nicolson method. It consists of discretizing the PDE with implicit trapezoid in time, and second order central difference in space (Gustafsson, 2007, p. 39). For simple one dimensional diffusion without advection, as given by equation (2.2), the Crank-Nicolson method describing the concentration of tracer particles is

$$\frac{C_n^{i+1} - C_n^i}{\Delta t} = \frac{K}{2\Delta x^2}(C_{n+1}^{i+1} - 2C_n^{i+1} + C_{n-1}^{i+1} + C_{n+1}^i - 2C_n^i + C_{n-1}^i), \tag{2.23}$$

where C is the concentration, i and n are the temporal and spatial indices respectively, Δt and Δx are the temporal and spatial discretization step sizes respectively, and K is the diffusivity. The method is second order and implicit in time. An important consideration when using FDMs is the stability of the method which describes the development of numerical error with the timestep size. Both the derivation of equation (2.23) and a proof of the stability of the method can be found in appendix A.

On the other hand, the random walk and random flight methods presented previously in sections 2.6 and 2.7 are examples of Lagrangian methods since these consider individual particle parcels rather than the flow field as a whole.

2.8.2 Boundary conditions

When doing both Eulerian and Lagrangian simulations one needs to consider what to do when particles cross a boundary of the spatial interval of interest. The topic of boundary conditions in Lagrangian models is not often discussed in the applied literature, and we are therefore interested in illumiating this topic in this thesis. In an FDM, the implementation of boundary conditions is usually accomplished by changing some of the values in the linear algebra system that is used to describe the method, while for stochastic particle methods we cannot a priori know if a particle will cross a boundary, and we therefore need an approach where we in some way change the particle position back to some acceptable value after it has stepped out of the acceptable domain. In this thesis we will only be considering systems with reflecting boundary conditions. For the stochastic particle methods we will consider

two different approaches to this; one simple method, and one more advanced method presented by Lépingle (1995).

Simple reflection

For some potential new position of a particle

$$\tilde{z}_{n+1} = f(z_n) \tag{2.24}$$

we want to check if the particle is outside the domain of interest $[0, L]$, and if so we reflect it back inside. If the particle is to the left of the domain ($\tilde{z}_{n+1} < 0$) meaning it has hit the water surface, the reflection simply consists of changing the sign of the position. If the position is to the right of the domain ($\tilde{z}_{n+1} > L$) meaning it has hit the ocean floor, the reflection is carried out by subtracting $\tilde{z}_{n+1}$ from $2L$. If the particle is within the domain, nothing is done. This method depends on a sufficiently large domain size L compared to the step sizes Δz so that the particle is never a distance greater than L outside the domain on either side, since in such a case this reflection scheme would simply move the particle from being outside the domain on one side to being outside it on the other. The actual new position z_{n+1} can then be expressed as

$$z_{n+1} = \begin{cases} -\tilde{z}_{n+1} & \text{if } \tilde{z}_{n+1} < 0 \\ 2L - \tilde{z}_{n+1} & \text{if } \tilde{z}_{n+1} > L \\ \tilde{z}_{n+1} & \text{otherwise} \end{cases} \tag{2.25}$$

When this scheme is applied to the random flight method, with some potential new velocity $\tilde{v}_{n+1} = f(z_n, v_n)$, the reflected velocity simply changes its sign such that it travels at the same speed but in the opposite direction after the reflection:

$$v_{n+1} = \begin{cases} -\tilde{v}_{n+1} & \text{if } \tilde{z}_{n+1} < 0 \text{ or } \tilde{z}_{n+1} > L, \\ \tilde{v}_{n+1} & \text{otherwise.} \end{cases} \tag{2.26}$$

Lépingle reflection

Since our Lagrangian models are constrained by using a finite timestep Δt we are faced with the possibility that a particle that is inside the valid domain at both times t and $t + \Delta t$ might have gone outside it at a time in the sub-interval between t and $t + \Delta t$. An illustration of this can be seen in figure 2.4 where we see that one of the possible trajectories between the two points crosses the reflecting boundary. This is the motivation for introducing a new reflection scheme. Given some potential new

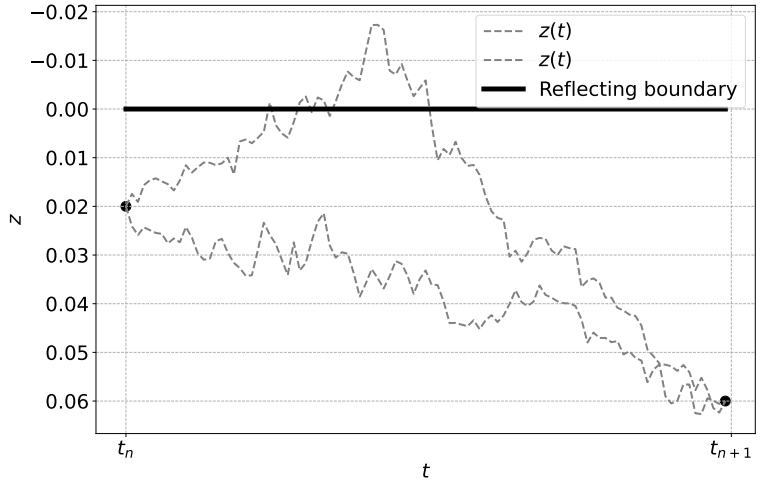

Figure 2.4: An illustration of two possible trajectories, $z(t)$, between the points (t_n, z_n) and (t_{n+1}, z_{n+1}). Even if the particle is inside the domain at these points, it might still have been outside between.

position, $\tilde{z}_{n+1}$, as in equation (2.24), the Lépingle reflection scheme can be written as

$$z_{n+1} = \tilde{z}_{n+1} + \max(0, A_n - z_n) \tag{2.27}$$

where

$$A_n = \frac{1}{2}[-a(z_n)\Delta t - b(z_n)\Delta W_n + \sqrt{b(z_n)^2 V_n + (-a(z_n)\Delta t - b(z_n)\Delta W_n)^2}] \tag{2.28}$$

Here $a(z_n) = K'(z_n)$ and $b(z_n) = \sqrt{2K(z_n)}$ are the drift- and diffusion coefficients respectively, and V_n is an exponential random variable with rate parameter $\lambda = (2\Delta t)^{-1}$. The inclusion of this exponential variable is motivated by the observation that the distance outside the acceptable domain traveled by a particle between two timesteps is exponentially distributed, with it being exponentially less likely for a particle to move to a point outside the domain the further away that point is.

2.9 Monte Carlo error

When trying to glean insight into the development of macroscopic quantities like concentration from statistical aggregation of microscopic quantities like position, the number N_p of tracked particles greatly affects the accuracy of these aggregations. The error we expect from using too few particles; or in other words an N_p that is too small, is called the Monte Carlo error.

Calculating the concentration for a sample of N_p positions is done by making

a histogram of the positions, which consists of subdividing the spatial interval of interest into a set of bins and counting the number of particles within each bin before doing the required normalization. Since the resulting positions from both the random walk and random flight simulations are stochastic variables, this counting of points that are internal to each bin is equivalent to doing a Monte Carlo integration (see e.g. Press et al. (2007, pp. 397-402)) of an indicator function that evaluates to 1 inside the bin and 0 elsewhere. For a given bin $[z_i, z_{i+1})$ the indicator function can be expressed as

$$f_i(z) = \begin{cases} 1 & \text{if } z_i \leq z < z_{i+1}, \\ 0 & \text{otherwise.} \end{cases} \tag{2.29}$$

The proportion of particles that are inside the i-th bin can then be expressed as

$$Q_i = \frac{1}{N_p} \sum_{j=0}^{N_p-1} f_i(z_j), \tag{2.30}$$

where N_p is the total number of tracked particles and z_j is the j-th position sample. This is equivalent to taking the mean of the function f_i evaluated on the points z_j. A suitable estimate for the error of this method of aggregation could be the standard deviations associated with this mean. Since this is a mean of stochastic variables, the central limit theorem gives a nice closed form for the standard deviation. Before doing the final step in deriving the Monte Carlo error, we will give a short presentation of the central limit theorem.

2.9.1 Central limit theorem

The central limit theorem states that for a set of stochastic variables $X_0, X_1, ..., X_{n-1}$ selected from a population with mean μ and finite standard deviation σ, with sample mean

$$\bar{X} \ = \frac{1}{n} \sum_{i=0}^{n-1} X_i, \tag{2.31}$$

the empirical standard deviation of the mean is

$$\sigma_{\bar{X}} \ = \frac{\sigma}{\sqrt{n}}. \tag{2.32}$$

This means that the empirical standard deviation of the sample mean $\bar{X}$ is expected to decrease with the inverse of the square root of the number of samples, meaning if we want to reduce the error by a factor of $\frac{1}{2}$ we need to increase the number of points n by a factor of 4.

2.9.2 Final thoughts on Monte Carlo error

Leveraging the central limit theorem presented above, using $\bar{X} = Q_i$, $n = N_p$, and

$$X_0, X_1, ..., X_{n-1} = f_i(z_0), f_i(z_1), ..., f_i(z_{N_p-1})$$

we find that the error, expressed through the standard deviation of the mean, is

$$\sigma_{Q_i} = \frac{\sigma}{\sqrt{N_p}}. \tag{2.33}$$

A short illustrative example can be made where we have some known probability distribution and draw N_p samples from this distribution. If we for instance represent the Monte Carlo error by the root-mean-square difference between the histogram values of the sample and the expected value found from evaluating the probability density function (PDF) of the population distribution at the relevant bin centers, we will observe that as N_p increases the error decreases.

We will illustrate this by taking samples from a Laplace distribution whose PDF is given by

$$p(x) = \frac{1}{2}e^{-|x|}. \tag{2.34}$$

Figure 2.5 shows how the sample histograms much more faithfully aligns with the expected values from the PDF for the bigger value of N_p, while figure 2.6 illustrates how the sample error falls like $\frac{\sigma}{\sqrt{N}}$, where σ is the known standard deviation of the Laplace distribution in equation (2.34).

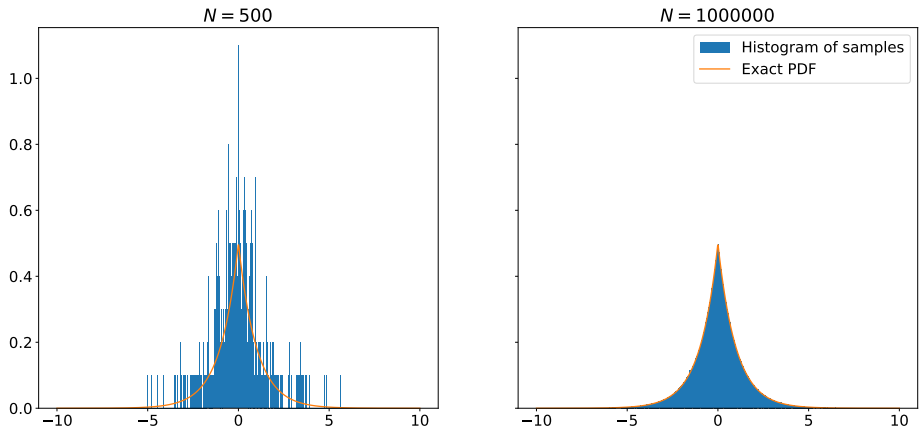

Figure 2.5: Two examples where we have drawn $N = 500$ and $N = 10^6$ samples from a Laplace distribution; both shown against the expected values given by the PDF.

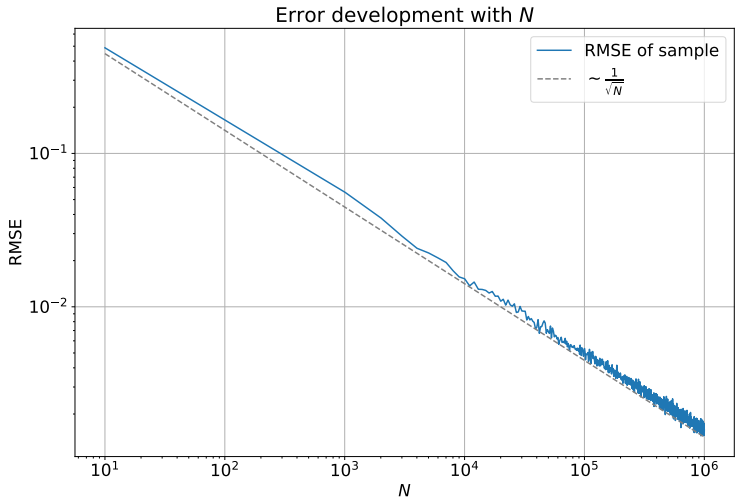

Figure 2.6: The root mean square error of the samples compared to the PDF plotted against the line proportional to $\frac{1}{\sqrt{N}}$ on a logarithmic plot.

2.10 Well-mixed condition

A common metric for the suitability of a Lagrangian model to simulate diffusion is called the well-mixed condition (WMC). It states that for a diffusion problem any initially well-mixed system, for instance meaning that the tracer particles starts evenly spread out, the system should always remain well mixed, given that the tracer can not move outside the system and that the diffusion is greater than zero everywhere (Thomson, 1987). This expectation can be seen directly from the diffusion equation (2.2): If the system is in a well-mixed state, as outlined above, where the particles are evenly distributed the spatial derivative of the concentration becomes zero

$$\frac{\partial C}{\partial z} = 0. \tag{2.35}$$

Inserting this into the right-hand side of equation (2.2) it immediately follows that

$$\frac{\partial C}{\partial t} = 0, \tag{2.36}$$

meaning that concentration is stationary and does not change with time. The physical intuition for this can be linked to the concept of entropy: A well mixed state where all particles are evenly distributed has the highest possible entropy of that system, and given a simple closed system, the second law of thermodynamics tells us that the entropy cannot decrease, which in our case would mean the system going from a well-mixed state to one that is not well-mixed. The famous example of non-decreasing entropy where we are mixing milk in our tea is illustrative of this since

it is also an example of a system of turbulent diffusion: If we consider the state of the milk being well dispersed in the tea due to our stirring with a teaspoon to be a well-mixed state, we know from experience that no amount of stirring will unmix the milk from the tea, and thus this token turbulent system will remain well-mixed.

2.11 Convergence

An interesting property of stochastic particle models is the convergence of the method. Just like for PDE solvers, this is a measure of how rapidly the method approaches the "true" solution as we decrease the timestep Δt. However, due to the stochastic nature of SDEs the concept of convergence differs from that of PDEs: For SDEs we have two different concepts of convergence, namely weak and strong. A stochastic method is said to have convergence of order γ if for sufficiently small Δt there exists a Λ such that

$$|\langle p(X_n)\rangle - \langle p(X(t))\rangle| \leq \Lambda \Delta t^{\gamma} : \text{weak} \tag{2.37}$$

$$\langle |X_n - X(t)|\rangle \leq \Lambda \Delta t^{\gamma} : \text{strong}, \tag{2.38}$$

for $t = n \cdot \Delta t \in [0, T]$ (Gräwe et al., 2012). Here, $X(t)$ represents the exact solution at time t and X_n is the approximation (this is opposite of the notation used in the source, but the equation remains the same), and $p(\cdot)$ is some polynomial function. Also note that Λ is an unknown parameter which is dependent on the equation we are trying to solve, while γ should only depend on the method used: The parameter Λ is therefore not of much interest when determining the order of convergence. Weak convergence, as given by equation (2.37), then relates to the statistical moments of the distribution of particle positions. This means that we are looking for how the mean, variance, skewness etc. converge. Strong convergence, on the other hand, concerns how each individual particle trajectory converges, and weak convergence is therefore implied if strong convergence is present.

Chapter 3

Method

In this chapter we will look at the methodology used to investigate stochastic particle methods for diffusion problems in breaking waves. All the simulations have been done using the Python programming language, and the code used can be found in my public Git repository [1].

3.1 Simulation setup

The main variables that describe the systems that we will simulate are the initial distributions for both position and velocity, the depth of water that is simulated, as well as the diffusivity profile. As we are mostly interested in the behaviour of the paricles near the surface, we consider a water column of depth $L = 2$ m in all simulations, and use positive z-direction downwards. Using $z = 0$ at the surface, this means that we consider the interval $z \in [0, L] = [0 \text{ m}, 2 \text{ m}]$ in all simulations.

3.1.1 Initial position distributions

For the initial position distributions we use three different distributions; the uniform distribution, Dirac delta distribution, and truncated normal distribution. Figure 3.1 shows all three position distributions used, and a more detailed description of each distribution follows below.

Uniform distribution A uniform distribution on a given interval $\mathcal{U}(a, b)$ means it is equally likely for a particle to occupy any position in that interval. For our case

[1] https://codeberg.org/konki/Masterprosjekt

with the interval [0 m, 2 m] the PDF of the distribution reads

$$p(x) = \begin{cases} \frac{1}{2} & 0 \leq x \leq 2, \\ 0 & \text{otherwise.} \end{cases} \tag{3.1}$$

It represents an even distribution of the particles, and we use it here to initialize systems as well-mixed. In general, the mean and variance of this distribution on the interval $[a, b]$ is $\mu = \frac{b-a}{2}$ and $\sigma^2 = \frac{(b-a)^2}{12}$ respectively, which on our interval gives $\mu = 1$ and $\sigma^2 = \frac{1}{3}$. In the code this initial distribution is achieved using the following code

```
import numpy as np

Np = 10_000_000                 # Number of particles to be simulated.
L = 2                           # Depth of water column in meters.

z0 = np.random.uniform(0, L, size=Np) # Initial position distribution.
```

Dirac delta distribution The Dirac delta distribution $\delta(x)$ is infinite in a single point and zero everywhere else, meaning the only place one could find a particle is that specific point. Its PDF is

$$\delta(x) = \begin{cases} \infty & x = 0, \\ 0 & \text{otherwise,} \end{cases} \tag{3.2}$$

but numerically this position distribution is achieved simply by initializing all particles at the same position, skipping the step of drawing them from a distribution all together. My code simply reads

```
import numpy as np

Np = 10_000_000             # Number of particles to simulate.
L = 2                       # Depth of water in meters.
loc = L / 2                 # Desired location where all particles are
                            # initialized, in this case in
                            # the middle of the domain.

z0 = np.repeat(loc, repeats=Np) # Initial position distribution.
```

Equation (3.2) describes a system where all particles are initialized at zero, but one can easily initialize at any arbitrary point a by doing the substitution $x \to x - a$.

Truncated normal distribution The normal distribution $\mathcal{N}(\mu, \sigma^2)$ is a well-studied distribution and its PDF reads

$$p(x) = \frac{1}{\sigma\sqrt{2\pi}} e^{-\frac{1}{2}(\frac{x-\mu}{\sigma})^2} \tag{3.3}$$

One of its properties is that the PDF evaluates to a non-zero value everywhere (save for the cases where $\sigma^2 = 0$, in which case the normal distribution is simply a Dirac delta distribution like the one presented above). This means that to be able to use this as an initial particle distribution within our domain $[0, L]$ we need to modify the distribution to a so-called truncated normal distribution. To this end we modify the PDF to evaluate to zero everywhere outside the domain, and rescale the function inside the domain to still integrate to 1. In the code this is done using the method `truncnorm` form the library `scipy`:

```
import numpy as np
from scipy.stats import truncnorm

Np  = 10_000_000                    # Number of particles to simulate
L   = 2                             # Depth of water in meters
std = 0.5                           # Standard deviation of the
                                    # distribution
loc = L / 2                         # Center of the normal distribution
                                    # in this case in the middle of the
                                    # domain

# Edges of the domain in number of standard deviations from the mean
a, b = (0 - loc) / std, (L - loc) / std

# Initial position distribution
z0 = truncnorm.rvs(a, b, loc=loc, scale=std, size=Np)
```

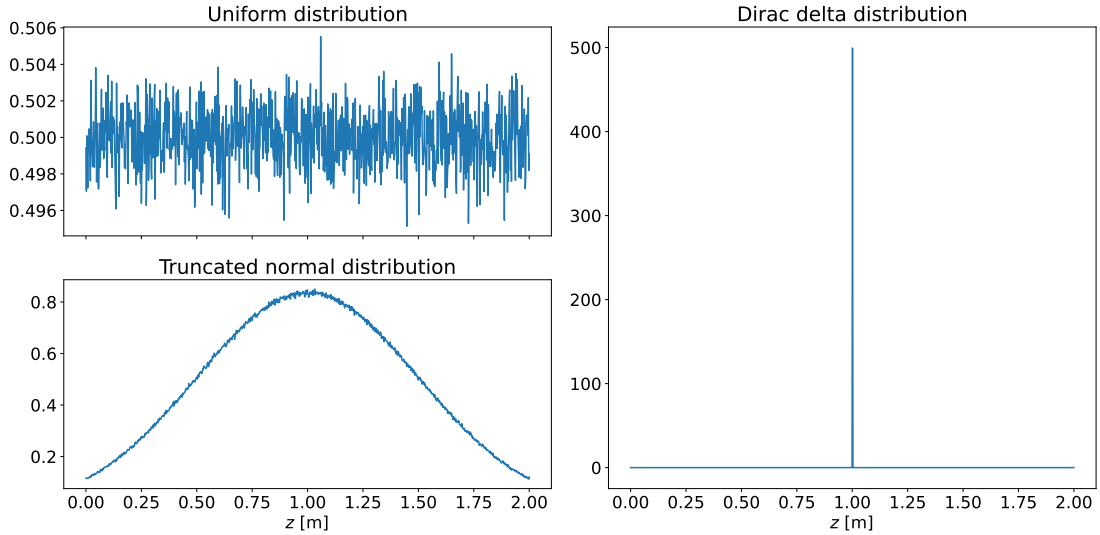

Figure 3.1: The different initial position distributions used. Note the different scales on the vertical axes.

3.1.2 Diffusivity profiles

The diffusivity profile of the water column describes the degree to which mixing is happening as a function of position and/or time. Since our simulations do not track time explicitly as a variable but only implicitly through the timestep Δt, we limit our scope to only consider diffusivity profiles that are stationary; that is they do not change with time.

In the following simulations we will use a diffusivity profile that decays linearly towards the surface, and exponentially for large depths

$$K(z) = K_0 + K_1 z e^{-\alpha z}, \tag{3.4}$$

where we use $K_0 = 2 \cdot 10^{-4}$ m^2/s, $K_1 = 2 \cdot 10^{-3}$ m/s, and $\alpha = \frac{1}{L} = 0.5$ m^{-1}. As we will only consider a domain of $z \in [0\text{ m}, 2\text{ m}]$, the effects of the exponentially decaying term will be minimal. The derivative of this function, which is used in the update formula for the random walk shown in equation (2.13) is

$$K'(z) = K_1 e^{-\alpha z} \cdot (1 - \alpha z). \tag{3.5}$$

For simpler simulations we sometimes use a constant diffusivity profile which reads

$$K_{\text{const}}(z) = K_0 \tag{3.6}$$

and hence the derivative for the constant case is simply

$$K'_{\text{const}}(z) = 0 \tag{3.7}$$

Both the constant and variable diffusivity profiles and their derivatives can be seen in Figure 3.2

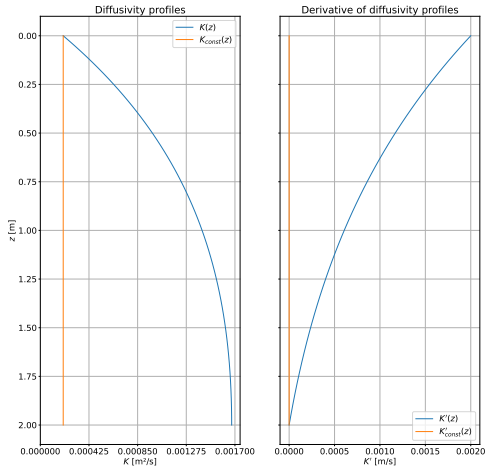

Figure 3.2: The different diffusivity profiles used and their derivatives

3.2 Convergence

We will look at both the strong and weak convergence for the random walk and random flight methods. In both the case of the weak and the strong convergence we need to run several realizations of the same simulations, only changing the timestep Δt, and comparing the final positions of the simulations to those of the exact solution. As we do not know the exact solutions we instead use the simulation with the reference timestep Δt_{ref} as a reference solution that the other simulations are compared to. To this end Δt_{ref} needs to be much smaller than the second-smallest timestep so that our reference solution can be considered to be significantly better than the other simulations that we will compare it to. Using equations (2.38) and (2.37), we can write the expression for the error of a single timestep size Δt_i

$$e_i = \begin{cases} \left| \langle p(Z^i_{(\text{final})}) \rangle - \langle p(Z^{ref}_{(\text{final})}) \rangle \right| & \text{weak,} \\ \left\langle \left| Z^i_{(\text{final})} - Z^{ref}_{(\text{final})} \right| \right\rangle & \text{strong.} \end{cases} \tag{3.8}$$

Remembering, from equations (2.37) and (2.38), that the requirement for convergence is

$$e(\Delta t) \leq \Lambda \Delta t^{\gamma}, \tag{3.9}$$

and taking the logarithm on both sides of the equality case of equation (3.9)

$$\log e(\Delta t) = \log \Lambda + \gamma \log \Delta t, \tag{3.10}$$

we can find the upper bound of the order by doing a linear regression with the results of the simulations

$$\log e_i = \log \Lambda + \gamma \log \Delta t_i \tag{3.11}$$

and solving for the order γ. Note, as mentioned earlier, that Λ is given by the equation we are trying to solve, and is therefore not of much interest when determining the order of convergence.

3.2.1 Convergence of trajectories

To investigate the strong convergence of the methods we are looking at how the *trajectories* of each particle converge to the trajectory of the reference solution as Δt decreases. To be able to achieve this the simulations need to use the same realization of the Wiener process, or else the simulations would not approximate the same trajectories. Remembering that the Wiener process is a function over time, we create a reference realization of W^{ref} with $\Delta t = \Delta t_{ref}$. For a simulation with timestep size $\Delta t_i = m \cdot \Delta t_{ref}$, with $m \in \mathbb{N}$, the value of ΔW_n^i at a given temporal position n can be found be finding the appropriate increment of the reference Wiener process $\Delta W_n^i = W_{n+m}^{ref} - W_n^{ref}$. By doing this, all ΔW^i represent the same trajectories, only with different temporal resolutions given by Δt_i. Figure 3.3 gives an illustrative example of what multiple realizations of the same Wiener process with different timesteps looks like.

Figure 3.3: Four realizations of the same Wiener process using different timesteps. The units on both axes are arbitrary.

Chapter 4

Results and discussion

In this chapter we present the results obtained together with discussions of these results.

4.1 Random walk and random flight

4.1.1 Monte Carlo error

To investigate the development of the Monte Carlo error one should fix all parameters of the system, except the number of particles N_p, and run a series of simulations with an increasing number of particles and investigate the distribution of positions at the end time T. Since we do not know what the "true" position distribution of the particles should be, which is needed for the error-calculation, we instead use the sample with the highest N_p as the benchmark that the other samples are measured against using the root-mean-square error.

As we can see in Figure 4.1 the Monte Carlo error for both the random flight and random walk behave in the way we expect according to the theory presented previously. As the errors of both methods follow each other so closely we can conclude that the choice of N_p is equally important for both methods.

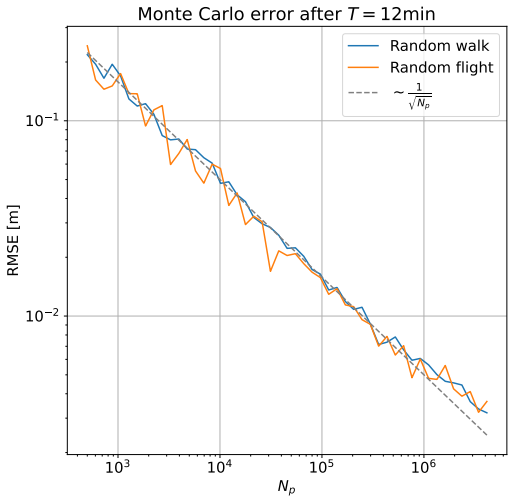

Figure 4.1: Development of the Monte Carlo error for both random flight and random walk.

4.1.2 Convergence

Strong convergence

To investigate the strong convergence of the random walk and random flight methods we simulate $N_p = 4000$ particles, with reference timestep $\Delta t_{ref} = 2^{-8}$ s, and total simulation time $T = 512$ s. We simulate using timestep sizes

$$\Delta t \in \{2^n \Delta t_{ref} | n \in 3, ..., 11\}, \tag{4.1}$$

giving $N = 9$ different simulations. We use the variable diffusivity profile from equation (3.4) with the simple reflection scheme. All particle positions are initialized with a Dirac delta distribution at $z = \frac{L}{2} = 1$, and for the random flight, the velocity is initialized at 0.

The error for each timestep size Δt_i may be found by taking the mean absolute error of the position at the final timestep with respect to the reference solution

$$e_i = \text{MAE} = \langle \left| Z^i_{(\text{final})} - Z^{ref}_{(\text{final})} \right| \rangle \tag{4.2}$$

As we can see from figure 4.2 random walk has a strong convergence of order $\gamma \approx 0.51$. This is in line with what we know from the literature about the Euler-Maruyama scehme which is order $\gamma = \frac{1}{2}$ (Gräwe et al., 2012). We can also see that the random flight method has a similar order convergence with $\gamma = 0.47$, though it has an overall higher error than the random walk for the timestep sizes we have considered here.

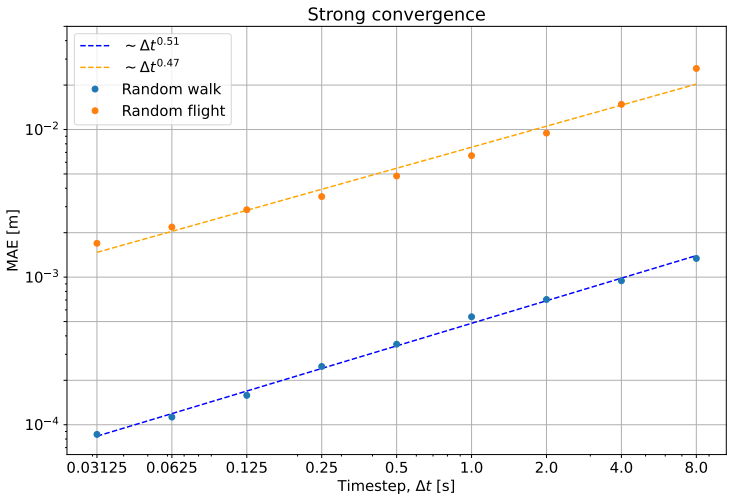

Figure 4.2: Strong convergence of random walk and random flight. The dashed lines are the linear regression of the random walk and random flight respectively.

These simulations used the constant diffusivity profile, which means that $K'(z) = 0 \quad \forall z \in \mathbb{R}$. If we apply this to the Langevin equation for the random walk in equation (2.6), we see that the only term that directly relies on the timestep, $\sqrt{2K'(z)}\Delta t$, vanishes. The only dependence of this equation on the timestep is then contained in the increment of the Wiener process, $\Delta W_n = \mathcal{N}(0, \Delta t)$, but since we are comparing trajectories using the same realization of the Wiener process we would expect all the particles to have the same final position, and therefore for the error to be constant and (almost) zero. This would be the case in the absence of a reflecting boundary, as demonstrated in figure 4.3. This shows that the error we observe in the random walk is purely a result of the reflecting boundaries, but since the convergence order of the random flight method remains the same even without boundaries it is clear that the same is not true for this method. Considering that the Langevin equation for the random flight in equation (2.14) does not depend on $K'(z)$, this behavior is in line with what we would expect.

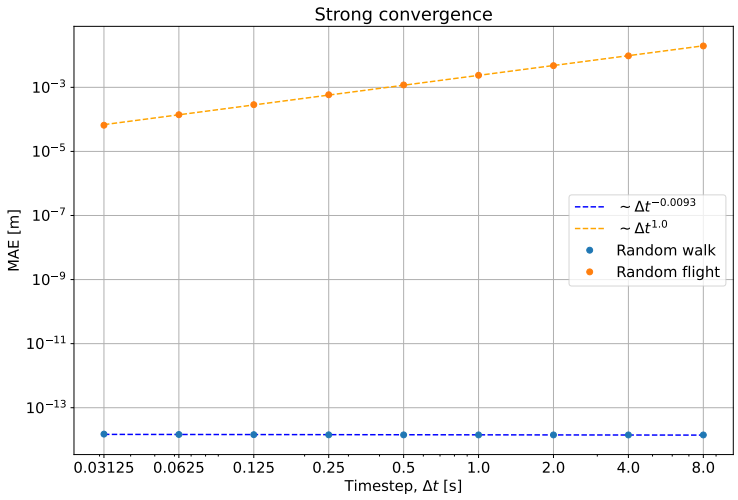

Figure 4.3: Strong convergence if no reflecting boundary is applied.

Weak convergence

As weak convergence relates to how the *moments* of the samples converge to the reference solution we need to simulate many more particles than what we needed for checking the strong case. To this end we use $N_p = 40000$, $\Delta t_{ref} = 2^{-4}$ s, and Δt as in equation (4.1). The moments we will consider are the mean and the variance of the distribution, and using the absolute error of the final distribution resulting from timestep size Δt_i as a measure of the error, which becomes

$$e_i = \text{AE} = \left| \langle Z^i_{(\text{final})} \rangle - \langle Z^{ref}_{(\text{final})} \rangle \right| \qquad \text{mean,} \tag{4.3}$$

$$e_i = \text{AE} = \left| \text{Var}(Z^i_{(\text{final})}) - \text{Var}(Z^{ref}_{(\text{final})}) \right| \qquad \text{variance.} \tag{4.4}$$

If we first consider the convergence with respect to the position mean as shown in the figure on the left in figure 4.4 it is clear that both models scale well with Δt which implies a convergence of order $\gamma = 1$. This is again in line with what we expect from the literature, where we know the Euler-Maruyama scheme to be of weak order $\gamma = 1$.

When considering the variance we can see from the figure on the right that the random flight still follows Δt very well, as does the random walk for larger timestep sizes, but for small timestep sizes it becomes apparent that the number of particles $N_p = 40000$ was not adequate to capture the weak convergence of the random walk method.

Still we notice that the overall error of the random flight method is significantly higher than that of the random walk, and since they are of the same order in the

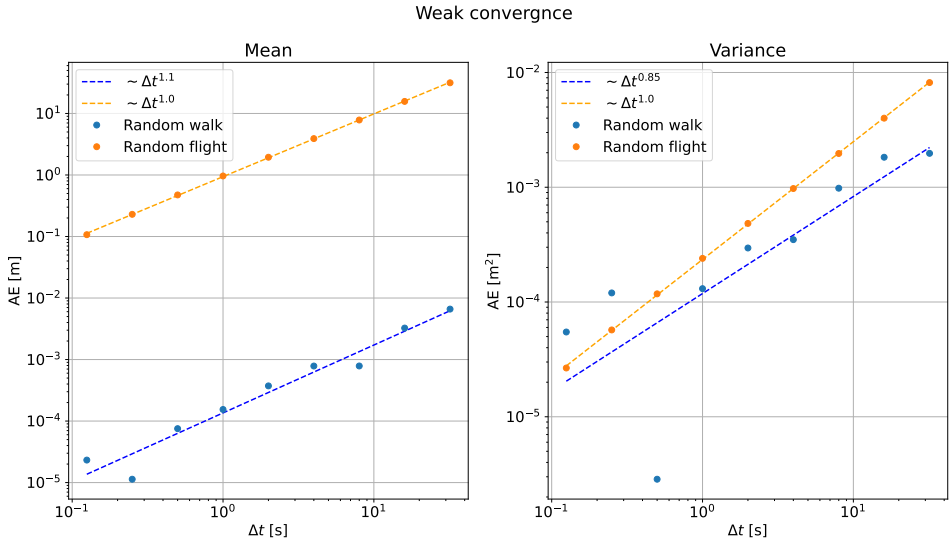

Figure 4.4: Convergence of mean and variance of particle positions.

weak sense, we cannot make the former more precise than the latter by choosing more appropriate timesteps.

4.2 Impact of reflection schemes

We will now investigate the impact of the reflection scheme on the random walk method.

4.2.1 Well-mixed condition

An important thing to do after implementing a numerical method is to check if it satisfies the WMC, as this is a necessary requirement for the method to be a faithful representation of diffusion. We check this by creating a uniform distribution of the particle positions z within the domain $[0, L]$, and running the simulations for a total time $T = 6$ h with the different combinations of reflection schemes and particle methods. We simulate $N_p = 5000000$ particles using the variable diffusivity profile from equation (3.4) and a timestep of size $\Delta t = 12$ s. For the random flight the initial velocity of all the particles are set to 0. After the simulation we investigate whether the distribution has changed in any meaningful way by comparing the mean and variance of the final distributions of each method to that of a perfectly uniform distribution.

The final position distributions after running the different simulations can be seen in figure 4.5. Here we can see that both random walk and random flight with the simple reflection scheme preserve the well mixed state of the system quite well, while

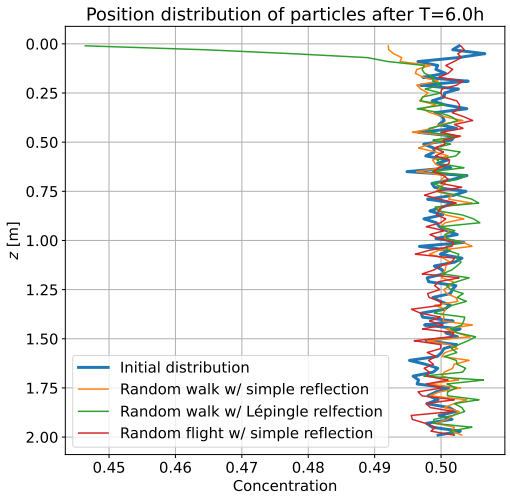

Figure 4.5: Position distributions after 6 hours for random walk with simple and Lépingle reflection schemes, as well as random flight with simple reflection scheme, all plotted against the initial position distribution.

the Lépingle reflection scheme produces a quite big deviation near the reflecting boundary at $z = 0$. This is further seen in table 4.1 where we can see that the Lépingle scheme has the highest error for both the mean and variance.

	$\langle \mathbf{Z} \rangle$	$\mathbf{Var(Z)}$	$\lvert \mathbf{1} - \langle \mathbf{Z} \rangle \rvert$	$\left\lvert \frac{\mathbf{1}}{\mathbf{3}} - \mathbf{Var(Z)} \right\rvert$
Initial distribution	0.999536	0.333383	$4.64 \cdot 10^{-4}$	$5.5 \cdot 10^{-5}$
Random walk w/ simple reflection	1.001850	0.332736	$1.85 \cdot 10^{-3}$	$5.98 \cdot 10^{-4}$
Random walk w/ Lépingle reflection	1.003749	0.331375	$3.75 \cdot 10^{-3}$	$1.96 \cdot 10^{-3}$
Random flight w/ simple reflection	0.998627	0.333491	$1.37 \cdot 10^{-3}$	$1.57 \cdot 10^{-4}$

Table 4.1: The first two columns are the mean and variance of the initial distribution as well as of the final distributions for all methods and reflection schemes. The last two columns are the deviation of these means and variances from the exact mean and variance of the uniform distribution.

4.2.2 Comparison with Crank-Nicolson method

Lastly we consider a comparison of the random walk method and the direct solution of the diffusion PDE by the Crank-Nicolson method. Both methods are well suited and widely used for simulation of diffusion. We are specifically interested in the behavior near a reflecting boundary where the derivative of the diffusivity is non-zero, as this is where we expect an artifact to occur, as discussed in the introduction (see also Ross and Sharples, 2004; Nordam et al., 2019). This is the case for the reflecting boundary at $z = 0$ with the variable diffusivity profile given in equation (3.4), and we therefore will give both methods the same initial position distribution near this boundary and compare their development over time. We will investigate how the choice of reflection scheme between simple and Lépingle reflection affect the results. The comparison consists of comparing the resulting concentrations from each method at each time and calculating the mean absolute error (MAE) as a representation of how much they differ, as well as a qualitative comparison of the concentrations at the end time T. We will also look at the weak convergence of the random walk with the different reflection schemes where we use the result from the Crank-Nicolson method as a reference solution.

The simulations are run using a total simulation time $T = 5$ min, varying timesteps, and using the variable diffusivity profile given in equation (3.4). The concentration is initialized as a truncated normal distribution centered at $z = 0.1L = 0.2$ m and with a standard deviation of $\sigma = 0.1$ m. For the random walk we use $N_p = 100000000$ particles, and for the Crank-Nicolson method we use a spatial discretization of size $\Delta x = \frac{L}{10000} = 0.0002$ m.

It is clear from figure 4.6 that the overall behavior of random walk with both

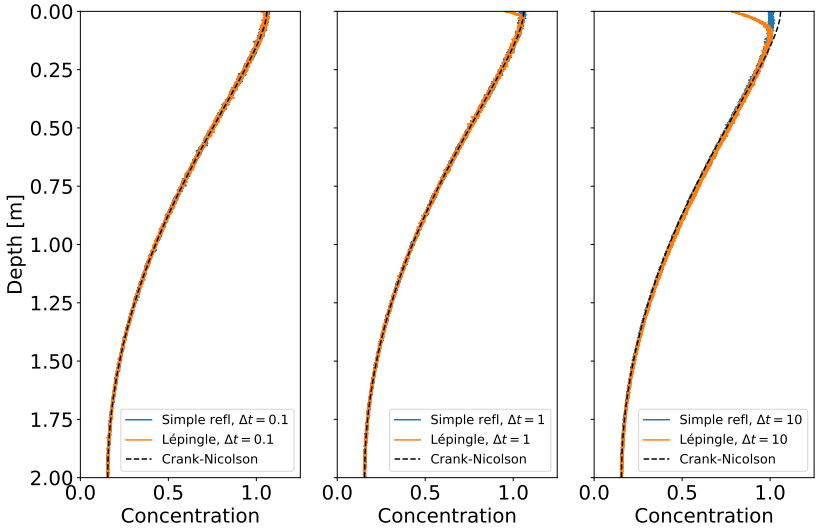

Figure 4.6: Concentration of particles resulting from the random walk and Crank-Nicolson methods at different times.

reflection schemes and the Crank-Nicolson method follow each other closely, but when inspecting the behavior near the surface boundary we observe rather large deviations for the Lépingle method and smaller deviations for the simple method. This is reflected in figure 4.7 where, when we consider mean absolute error, can see that the Lépingle method has consistently higher error than the simple method.

Furthermore, to investigate the weak convergence with the different reflection schemes we run the same simulation as above multiple times, only changing the timestep size and calculated the error in the first moment. Figure 4.8 considers the error in the first moment of the Lagrangian method relative to the Eulerian. The first moment is given by $\frac{1}{N_p}\sum_{i=0}^{N_p-1} z_i$ for the Lagrangian method and $\int_0^L zC(z)dz$ for the Eulerian, where we use Simpsons method to calculate the integral. As we can see from the figure the reflection schemes converge in the weak sense with order ~ 1.08 for simple and ~ 0.929 for Lépingle reflection.

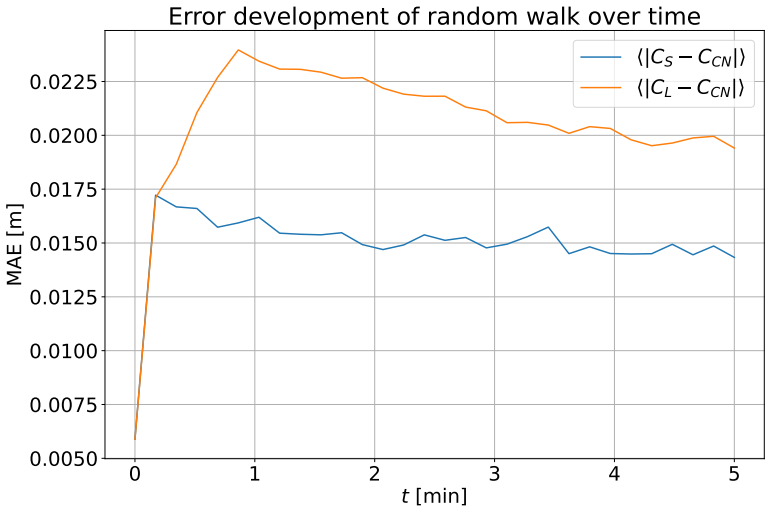

Figure 4.7: Time development of the mean absolute error between the concentrations resulting from the random walk with simple and Lépingle reflection (C_S and C_L) and Crank-Nicolson methods (C_{CN})

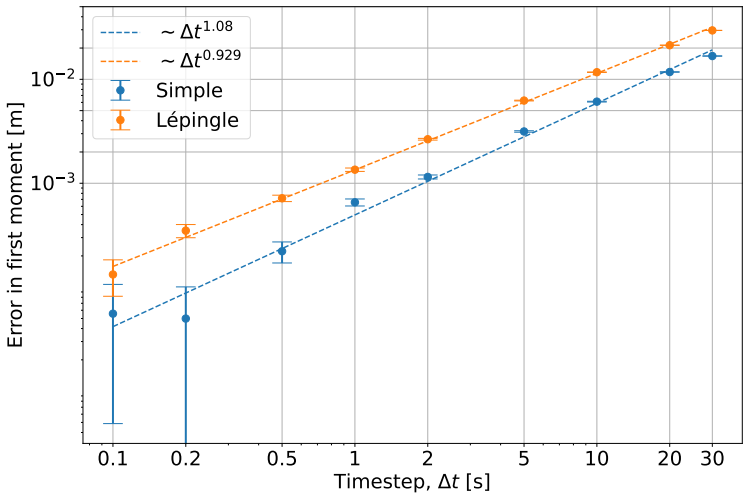

Figure 4.8: The convergence of random walk with simple and Lépingle reflection.

While Lépingle (1995) proves that his method has order of convergence $\frac{1}{2}$ in the strong sense, there has to the best of my knowledge been no investigations of his reflection scheme in an applied context. In applications, one is typically more concerned with weak convergence, as this describes how the concentration field converges. It is interesting that the Lépingle method apparently has slower convergence than the simple reflection scheme in this context. If we also note that we found the Lépingle scheme to have a poor ability to preserve the well-mixed state of a diffusion system, and keeping in mind its double computational cost compared to the simple scheme, we conclude that there seems to be no benefit, but rather a detriment, in choosing this method of reflection over the simple scheme.

Chapter 5

Conclusion

In this thesis we have investigated the differences and similarities of the random walk and random flight methods for simulation of diffusion, as well as the impact of choice of reflection scheme on the random walk method. We have found that both methods satisfy the well-mixed condition when using a simple reflection scheme, but that when using the Lépingle reflection scheme with the random walk method a large deviation appears near the reflecting boundary where the derivative of the diffusivity is zero.

The number of particles simulated plays a big role in the accuracy of a stochastic particle method, and the Monte Carlo error is an estimate of the error introduced to the system due to the choice of number of simulated particles. From the literature we would expect this to develop as one over the square root of the number of particles, which we have found to be the case for both the random walk and random flight.

Another important choice for the simulations is the size of the timestep. We have found that, using constant diffusivity and reflecting boundaries, the random walk method is of order ~ 0.51 in the strong sense and ~ 1.1 in the weak sense, while the random flight method is of order ~ 0.47, and ~ 1.0 respectively, while still maintaining a higher overall error that the random walk method.

Furthermore, we have found that, comparing the random walk with the different reflection schemes to the Crank-Nicolson method, the overall error when using the Lépingle method is significantly higher than that of the simple reflection scheme. Though Lépingle (1995) proves that his method is of order $\frac{1}{2}$ in the strong sense, one is often more interested in the weak convergence, as this relates to how the macroscopic property of concentration behaves. In this thesis we have found the Lépingle method to be of order ~ 0.929 in the weak sense, while the simple reflection method is of order ~ 1.08, making the former a poorer choice in this regard as well. Combining this with the fact that the Lépingle method has a higher computational cost, we conclude that the usage of this reflection scheme is a detriment rather than

a benefit to random walk method.

This leads us to conclude that due to it having little extra computational cost, the random flight method might be equally suitable for simulations of diffusion as the random walk method.

Bibliography

Abuhegazy, Mohamed et al. (Oct. 2020). 'Numerical investigation of aerosol transport in a classroom with relevance to COVID-19'. In: *Physics of Fluids* 32.10, p. 103311. ISSN: 1070-6631. DOI: 10.1063/5.0029118. URL: https://doi.org/10.1063/5.0029118 (visited on 15th May 2023).

Coffey, William and Yu P Kalmykov (2012). *The Langevin equation: with applications to stochastic problems in physics, chemistry and electrical engineering*. Vol. 27. World Scientific.

Einstein, Albert (1905). 'Über die von der molekularkinetischen Theorie der Wärme geforderte Bewegung von in ruhenden Flüssigkeiten suspendierten Teilchen'. de. In: *Annalen der Physik* 322.8, pp. 549–560. ISSN: 1521-3889. DOI: 10.1002/andp.19053220806. URL: https://onlinelibrary.wiley.com/doi/abs/10.1002/andp.19053220806 (visited on 11th May 2023).

Elliott, A. J., N. Hurford and C. J. Penn (1986). 'Shear diffusion and the spreading of oil slicks'. In: *Marine Pollution Bulletin* 17.7, pp. 308–313. ISSN: 0025-326X. DOI: https://doi.org/10.1016/0025-326X(86)90216-X. URL: https://www.sciencedirect.com/science/article/pii/0025326X8690216X.

Gillespie, Daniel T. (Aug. 1996). 'Exact numerical simulation of the Ornstein-Uhlenbeck process and its integral'. In: *Physical Review E* 54.2. Publisher: American Physical Society, pp. 2084–2091. DOI: 10.1103/PhysRevE.54.2084. URL: https://link.aps.org/doi/10.1103/PhysRevE.54.2084 (visited on 15th Apr. 2023).

Gillespie, Daniel T. and Effrosyni Seitaridou (Oct. 2012). *Simple Brownian Diffusion: An Introduction to the Standard Theoretical Models*. Oxford University Press. ISBN: 978-0-19-966450-4. DOI: 10.1093/acprof:oso/9780199664504.001.0001. URL: https://doi.org/10.1093/acprof:oso/9780199664504.001.0001.

Gräwe, Ulf et al. (Apr. 2012). 'Why the Euler scheme in particle tracking is not enough: the shallow-sea pycnocline test case'. en. In: *Ocean Dynamics* 62.4, pp. 501–514. ISSN: 1616-7228. DOI: 10.1007/s10236-012-0523-y. URL: https://doi.org/10.1007/s10236-012-0523-y (visited on 5th Mar. 2023).

Griffa, Annalisa (1996). 'Applications of stochastic particle models to oceanographic problems'. en. In: *Stochastic Modelling in Physical Oceanography*. Ed. by Robert

J. Adler, Peter Müller and Boris L. Rozovskii. Progress in Probability. Boston, MA: Birkhäuser, pp. 113–140. ISBN: 978-1-4612-2430-3. DOI: 10.1007/978-1-4612-2430-3_5. URL: https://doi.org/10.1007/978-1-4612-2430-3_5 (visited on 9th Apr. 2023).

Gustafsson, Bertil (2007). *High order difference methods for time dependent PDE*. Vol. 38. Springer Science & Business Media.

Kloeden, Peter M. (1992). *Numerical solution of stochastic differential equations*. 1st ed. Springer. DOI: https://doi.org/10.1007/978-3-662-12616-5. URL: https://link.springer.com/book/10.1007/978-3-662-12616-5#bibliographic-information.

Langevin, Paul (1908). 'Sur la théorie du mouvement brownien'. In: *Comptes Rendus de l'Académie des Sciences (Paris)* 146, pp. 530–533.

Lemons, Don and Anthony Gythiel (Jan. 1997). 'Paul Langevin's 1908 paper "On the Theory of Brownian Motion"'. In: *American Journal of Physics - AMER J PHYS* 65, pp. 1079–1081.

Lépingle, D. (May 1995). 'Euler scheme for reflected stochastic differential equations'. en. In: *Mathematics and Computers in Simulation* 38.1, pp. 119–126. ISSN: 0378-4754. DOI: 10.1016/0378-4754(93)E0074-F. URL: https://www.sciencedirect.com/science/article/pii/0378475493E0074F (visited on 27th Mar. 2023).

Lynch, Daniel R et al. (2014). *Particles in the coastal ocean: Theory and applications*. Cambridge University Press.

NobelPrize.org (2023). *The Nobel Prize in Physics 1926*. en-US. URL: https://www.nobelprize.org/prizes/physics/1926/summary/ (visited on 11th May 2023).

Nordam, Tor et al. (2019). 'Numerical analysis of boundary conditions in a Lagrangian particle model for vertical mixing, transport and surfacing of buoyant particles in the water column'. In: *Ocean Modelling* 136, pp. 107–119.

Onink, Victor et al. (June 2021). 'Global simulations of marine plastic transport show plastic trapping in coastal zones'. en. In: *Environmental Research Letters* 16.6. Publisher: IOP Publishing, p. 064053. ISSN: 1748-9326. DOI: 10.1088/1748-9326/abecbd. URL: https://dx.doi.org/10.1088/1748-9326/abecbd (visited on 15th May 2023).

Perrin, J. (1909). *Mouvement brownien et réalité moléculaire*. Masson et Cie, Éditeurs. URL: https://books.google.no/books?id=U6weHQAACAAJ.

Press, William H et al. (2007). *Numerical recipes*.

Ross, Oliver N and Jonathan Sharples (2004). 'Recipe for 1-D Lagrangian particle tracking models in space-varying diffusivity'. In: *Limnology and Oceanography: Methods* 2.9, pp. 289–302.

Tayfun, Mehmet A. and Hsiang Wang (Aug. 1973). 'Monte Carlo Simulation of Oil Slick Movements'. EN. In: *Journal of the Waterways, Harbors and Coastal Engineering Division* 99.3. Publisher: American Society of Civil Engineers, pp. 309–

324. DOI: 10.1061/AWHCAR.0000197. URL: https://ascelibrary.org/doi/10.1061/AWHCAR.0000197 (visited on 11th May 2023).

Thomson, D. J. (July 1987). 'Criteria for the selection of stochastic models of particle trajectories in turbulent flows'. en. In: *Journal of Fluid Mechanics* 180. Publisher: Cambridge University Press, pp. 529–556. ISSN: 1469-7645, 0022-1120. DOI: 10.1017/S0022112087001940. URL: https://www.cambridge.org/core/journals/journal-of-fluid-mechanics/article/criteria-for-the-selection-of-stochastic-models-of-particle-trajectories-in-turbulent-flows/3175551812282ED52EE96C23E37EBBDE (visited on 28th Mar. 2023).

Thorpe, Steve A (2005). *The turbulent ocean*. Cambridge University Press.

Appendix A

Stability of Crank Nicolson method

The Crank-Nicolosn method is defined to solve PDEs on the form

$$\frac{\partial C}{\partial t} = F(C, x, t) \tag{A.1}$$

where we discretize forwardly in time

$$\frac{C_n^{i+1} - C_n^i}{\Delta t} = \frac{1}{2}(F(C_n^{i+1}, x_n, t_{i+1}) + F(C_n^i, x_n, t_i)) \tag{A.2}$$

Given the 1-D diffusion equation with constant diffusivity K

$$\frac{\partial C}{\partial t} = K\frac{\partial^2 C}{\partial x^2} \tag{A.3}$$

Inserting this into equation (A.2) using $F(C, x, t) = K\frac{\partial^2 C}{\partial x^2}$ we get

$$\frac{C_n^{i+1} - C_n^i}{\Delta t} = \frac{1}{2}(K\frac{\partial^2 C_n^{i+1}}{\partial x^2} + K\frac{\partial^2 C_n^i}{\partial x^2}) \tag{A.4}$$

This equation can then be discretized centrally in space to get the following fully discretized expression for the Crank-Nicolson method

$$\frac{C_n^{i+1} - C_n^i}{\Delta t} = \frac{1}{2}(K\frac{C_{n+1}^{i+1} - 2C_n^{i+1} + C_{n-1}^{i+1}}{\Delta x^2} + K\frac{C_{n+1}^i - 2C_n^i + C_{n-1}^i}{\Delta x^2}) \tag{A.5}$$

$$= \frac{K}{2\Delta x^2}(C_{n+1}^{i+1} - 2C_n^{i+1} + C_{n-1}^{i+1} + C_{n+1}^i - 2C_n^i + C_{n-1}^i) \tag{A.6}$$

Collecting terms that are the same in the temporal index, and using $\alpha = \frac{K\Delta t}{2\Delta x^2}$ we get

$$C_n^{i+1} - \alpha(C_{n+1}^{i+1} - 2C_n^{i+1} + C_{n-1}^{i+1}) = C_n^i + \alpha(C_{n+1}^i - 2C_n^i + C_{n-1}^i) \tag{A.7}$$

The stability of the method is analyzed using von Neumann analysis by substituting $C_n^i = \hat{C}_k^i e^{jkx_n}$ where j is the imaginary unit. Inserting this into equation (A.7) we get

$$\begin{aligned}&\hat{C}_k^{i+1} e^{jkx_n} - \alpha(\hat{C}_k^{i+1} e^{jk(x_n+\Delta x)} - 2\hat{C}_k^i e^{jkx_n} + \hat{C}_k^{i+1} e^{jk(x_n-\Delta x)}) \\ &- \hat{C}_k^i e^{jkx_n} - \alpha(\hat{C}_k^i e^{jk(x_n+\Delta x)} - 2\hat{C}_k^i e^{jkx_n} + \hat{C}_k^i e^{jk(x_n-\Delta x)}) = 0\end{aligned}$$

Using $e^{jk(x_n \pm \Delta x)} = e^{jkx_n} \cdot e^{\pm jk\Delta x}$ and dividing by e^{jkx_n} everywhere we get

$$\begin{aligned}&\hat{C}_k^{i+1} - \alpha(\hat{C}_k^{i+1} e^{jk\Delta x} - 2\hat{C}_k^i + \hat{C}_k^{i+1} e^{-jk\Delta x}) \\ &- \hat{C}_k^i - \alpha(\hat{C}_k^i e^{jk\Delta x} - 2\hat{C}_k^i + \hat{C}_k^i e^{-jk\Delta x}) = 0\end{aligned}$$

Collecting terms, and using the identity $e^{j\theta} + e^{-j\theta} = 2\cos\theta$ we get

$$\hat{C}_k^{i+1}(1 + 2\alpha(1 - \cos k\Delta x)) - \hat{C}_k^i(1 - 2\alpha(1 - \cos k\Delta x)) = 0 \tag{A.8}$$

Solving for $\hat{C}_k^{i+1}$ gives

$$\hat{C}_k^{i+1} = \frac{1 - 2\alpha(1 - \cos k\Delta x)}{1 + 2\alpha(1 - \cos k\Delta x)} \hat{C}_k^i \tag{A.9}$$

This gives us the amplification factor

$$g(k\Delta x) = \frac{1 - 2\alpha(1 - \cos k\Delta x)}{1 + 2\alpha(1 - \cos k\Delta x)} \tag{A.10}$$

Since the denominator of equation (A.10) is always greater than or equal to the enumerator, the equation satisfies $|g(k\Delta x)| \leq 1$ which is the criterion for stability. This means that the method is unconditionally stable for the diffusion equation.